Scientia Iranica B (2021) 28(6), 3232–3245

Sharif University of Technology
Scientia Iranica
Transactions B: Mechanical Engineering
http://scientiairanica.sharif.edu

Damage propagation prediction of adhesion failure in composite T-joint structure and improvement using PZT patch

S.K. Panda[a], P.K. Mishra[a], and S.K. Panda[b,*]

a. *Department of Mechanical Engineering, CAPGS, BPUT, Rourkela, Odisha, India.*
b. *Department of Mechanical Engineering, National Institute of Technology, Rourkela, Odisha, India.*

Received 31 October 2020; received in revised form 27 December 2020; accepted 12 April 2021

KEYWORDS
Adhesion failure;
Laminated composite structure;
Piezoelectric material;
Strain energy release rate;
T-joint structure;
Virtual crack closure technique.

Abstract. This study develops a three-dimensional finite element simulation model for the prediction, propagation, and improvement of adhesion failure in an adhesively bonded laminated T-joint structure using smart piezoelectric materials. Initially, three-dimensional stresses (normal and shear) and failure locations in the composite T-joint (all the layers of the web and flange) were evaluated. In the identified failure location, Virtual Crack Closure Technique (VCCT) of fracture mechanics was employed to compute the Strain Energy Release Rate (SERR) values for different pre-embedded adhesion failure lengths. The developed coupling analysis model was employed to evaluate the SERR responses for the laminated composite T-joint with single/multiple piezoelectric layers. The efficacy and improved performance (resistance to adhesion failure) of the laminated smart T-joint structure were analyzed in detail by considering different influencing parameters, i.e., orientation schemes, material types, piezoelectric layers, thicknesses, and number of laminate layers.

1. Introduction

Adhesion/delamination is one of the most common modes of failure in laminated composite (plate, shell, and joints) structures. This mode of failure is too difficult to identify and capable of doing serious damage to any type of laminated structures. Therefore, it is very important to identify the exact failure location and provide resistance to the propagation of failure. Laminated composite structures have gained significant attention among researchers because of a wide range of applications in vital research fields [1–11]. The mechanical and electric properties of these laminated composite structures can be further enhanced by attaching smart piezoelectric layers and they together form a smart laminated composite structure. These smart structures integrated with piezoelectric sensors and actuators are widely used in different engineering applications. The piezoelectric actuators and sensors can be easily bonded to the surface of the base beam/plate structures as they are available in thin patches and composite forms. These kinds of structures are suitable for low frequency vibration control [12]. Therefore, many researchers have considered these smart structures integrated with sensors and actuators in real-time engineering problems like vibration control and shape control, energy harvesting, structural health monitoring, etc.

Laminated composite structures are very much

*. *Corresponding author. Tel.: +91-9658583368*
E-mail addresses: subhransupanda3@gmail.com (S.K. Panda); capgs.pkmishra@bput.ac.in (P.K. Mishra); call2subrat@gmail.com, pandask@nitrkl.ac.in (S.K. Panda)

doi: 10.24200/sci.2021.57083.5064

prone to interlaminar failures that occur in between two anisotropic layers. The geometrical discontinuity arising in the structure leads to a significant increase in the interlaminar stress. This mode of failure is too difficult to identify because the structure does not fail completely; however, the strength of the structure is attenuated significantly [13]. In laminated structures, the strength of the structure is greater when the fibers are orientated in the longitudinal and lateral directions. Similarly, interlaminar stress is significant at the boundary of the structure when subjected to transverse loading conditions. Therefore, the formation of a crack in laminated structures depends largely on the type of loading. Based on fracture mechanics, there are three modes of delamination failure and the combination of these three modes can be characterized by Strain Energy Release Rate (SERR).

Researchers mainly focus on developing mathematical and analytical models to understand the effect of delamination on the electromechanical response of smart laminated structures attached to sensors and actuators. The electromechanical response to damage propagation can be characterized using these mathematical models. These mathematical models are helpful for damage detection and localization. Shear deformation theory and Griffith-type fracture criterion can be used to understand the elastic buckling and post buckling for a delaminated axially loaded beam/plate. Li and Qing [14] used the modified Hellinger-Reissner variational principle to analyze composite laminated shells. The presence of delamination reduces the natural frequency of any type of beam/plate structure [15,16].

Euler Bernoulli/Timoshenko beam theory is used to model piezoelectric-based energy harvesters for calculating the amount of energy generated [17]. Many researchers have also attempted to determine the factors that affect the effective power generation and efficiency of the harvesters. The performance and characteristics of laminated composite structures are directly affected by the presence of delamination [18]. Generally, delamination propagates under operational loadings, causing the failure of the structures. Therefore, different loading conditions have been used to understand the delamination growth in laminated composite structures [19,20]. It is also important to identify the location of failure initiation and calculate the quality of the laminated structure. Therefore, many mathematical models and methodologies have been proposed to identify damage initiation and assess the damage to the structure. Time and low frequency based methodologies and non-destructive techniques were successively used in [21–23]. Crack propagation also depends upon the material's ability to absorb energy. Therefore, in the case of rubber, the delamination damage propagation is low [24]. Usually, thin piezoelectric materials, namely lead zirconate titanate (PZT) and polyvinylidene fluoride (PVDF) patches, are considered as sensors to identify damage initiation. They are either bonded to the surface or embedded in composites for detecting the damage [25]. Attempts have been made to address the actuator debonding and its influence on actuation through numerical analyses [26].

Many authors have considered refined plate theory and first-order shear deformation theory like mathematical models for static, dynamic, and thermomechanical analyses of laminated composite structures and sandwich panels [27–31]. These models with some advancement can be further extended to conducting static and dynamic analyses of Functionally Graded (FG) sandwich plates and structures [32–34]. Similarly, these laminated composite structures and FG structures can be attached to piezoelectric materials, sensors, and actuators for damage detection, vibration, buckling, and bending analyses [35–39]. Furthermore, refined zig-zag theories and piezo-elasticity theories have also been considered for dynamic buckling vibration analysis of FG carbon nanotube reinforced composite structures attached to piezoelectric layers [40,41].

The existing researches have pointed to the scope of analysis model for the adhesion/delamination crack in the design of laminated composite structures (plate, shell, joints, etc.). The objective of the present work is to develop a coupling analysis model for the laminated composite T-joint with the piezoelectric layer(s) to minimize the SERRs. This model can consider debonding at the interface of the web and flange part of the T-joint to evaluate the SERRs. The efficacy and performance (resistance to adhesion failure) of the laminated smart T-joint structure are analyzed in detail by considering different orientation schemes, material types, piezoelectric layers, thicknesses, and number of laminate layers.

2. Modelling of adhesively bonded T-joint structure

The schematic diagram of the adhesively bonded composite T-joint structure is shown in Figure 1. All the geometrical dimensions of the joint are presented in Table 1. Four $[0/90]_s$ orthotropic laminates are

Table 1. Geometrical properties of the joint structure.

Length (L, in m)	Width (w, in m)	Thickness (t, in m)	Height (H, in m)
0.16	0.18	0.0025	0.16

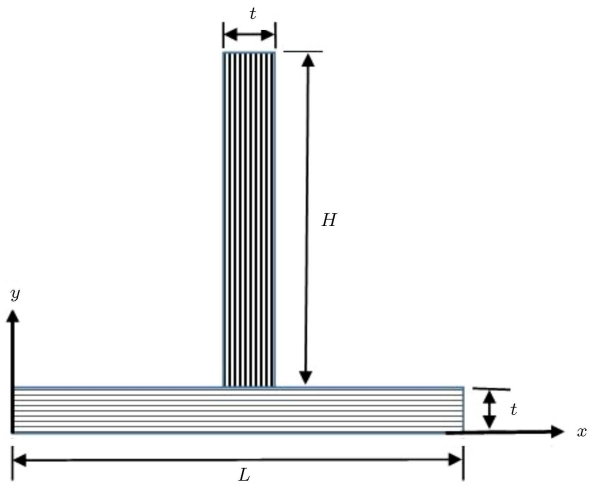

Figure 1. Schematic diagram of the laminated composite T-joint structure.

considered to model both the flange and web part of the T-joint structure. The layered solid 185 finite element type of Ansys Parametric Design Language (APDL) is used to model both the flange and web part of the T-joint.

The details of the material properties and corresponding strength values [42] are shown in Tables 2 and 3, respectively. A very finer mesh size (considering convergence solution) has been adopted to model the joint structure, as shown in Figure 2(a). The boundary and loading conditions of the joint structure are shown in Figure 2(b).

2.1. Stress analysis

In order to calculate the crack propagation in the laminated T-joint structure, it is important to understand the stress distributions. For this purpose, the stresses (normal and shear) have been calculated for all the layers of the flange and web part of the T-joint structure. Maximum stresses (both normal and shear) are found in the T-joint structure at (i) the interface of the flange and web and (ii) the bottom to the interface layer (1st layer of the flange), as shown in Table 4. However, out of the two locations, stresses are observed to be at a higher level at the interface of the flange and web compared to the 1st layer of the flange. It is also observed that the stress distributions (σ_{yy}, σ_{xy}, and σ_{xz}) are more prominent and lead to the adhesion/delamination failure in the joint structure.

2.2. Failure analysis

The stress components responsible for the adhesion/delamination damage propagation in the adhesively bonded T-joint structure are obtained from the stress analysis. By using these stress components and

Table 2. Mechanical properties of T300/934 carbon epoxy plain ply [42].

E_x (GPa)	E_y (GPa)	E_z (GPa)	G_{xy} (GPa)	G_{yz} (GPa)	G_{xz} (GPa)	ν_{xy}	ν_{yz}	ν_{xz}
57.226	57.226	4.480	4.481	4.400	4.400	0.050	0.280	0.280

Table 3. Strength values of T300/934 carbon epoxy plain ply [42].

X_t (MPa)	X_c (MPa)	Y_t (MPa)	Y_c (MPa)	Z (MPa)	S (MPa)
1270	1130	42	141	46	90

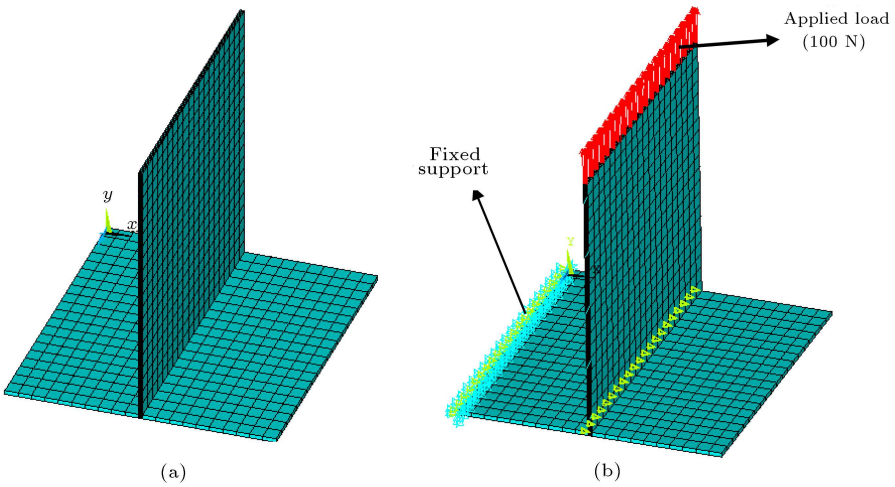

Figure 2. (a) Meshed view and (b) loading and boundary conditions of the joint structure.

Table 4. Maximum stress values for the first two layers of the joint structure.

Layer	σ_{xx} (N/m^2)	σ_{yy} (N/m^2)	σ_{zz} (N/m^2)	σ_{xy} (N/m^2)	σ_{yz} (N/m^2)	σ_{xz} (N/m^2)
Interface of the flange and web	1.5e2	1.5e7	1.0e2	1.2e7	7.5e6	1.0e7
Bottom to interface layer (1st layer of the flange)	1.2e2	5.2e6	0.6e2	8.0e6	6.4e6	1.2e6

their corresponding strength values in the Tsai-Wu quadratic failure criterion [43], the failure location in the joint structure can be identified.

$$\frac{\sigma_x^2}{X_c X_t}+\frac{\sigma_y^2}{Y_c Y_t}+\frac{\sigma_z^2}{Z_c Z_t}+\frac{\tau_{xy}^2}{S_{xy}^2}+\frac{\tau_{yz}^2}{S_{yz}^2}+\frac{\tau_{xz}^2}{S_{xz}^2}+\sigma_x\left(\frac{1}{X_t}-\frac{1}{X_c}\right)+\sigma_y\left(\frac{1}{Y_t}-\frac{1}{Y_c}\right)+\sigma_z\left(\frac{1}{Z_t}-\frac{1}{Z_c}\right)+f_{xy}\sigma_x\sigma_y+f_{yz}\sigma_y\sigma_z+f_{xz}\sigma_x\sigma_z=e^2\left\{\begin{array}{l} e<1, nofailure \\ e\geq 1, failure \end{array}\right\}. \quad (1)$$

Here, X_t, Y_t, and Z_t are the allowable principal tensile strengths in all three directions and S_{xy}, S_{yz}, and S_{xz} are the shearing strengths in different coupling modes of the orthotropic layer. Similarly, f_{xy}, f_{yz}, and f_{xz} are the coupling coefficients in the three principal directions.

In the present analysis, from the stress distribution, it is found that the normal stress in the y-direction (σ_y) has been more dominant. So, the damage initiation can be predicted by considering the normal stress component (σ_y) and the inter-laminar shear stress components (τ_{xy}, τ_{yz}) in the y-direction.

$$\left(\frac{\sigma_y}{Z}\right)^2+\left(\frac{\tau_{xy}}{S}\right)^2+\left(\frac{\tau_{yz}}{S}\right)^2=e^2\left\{\begin{array}{l} e<1, nofailure \\ e\geq 1, failure \end{array}\right\}, \quad (2)$$

where Z is the inter-laminar normal strength and S is the inter-laminar shear strengths which are considered to be equal, i.e., $S_{xy}=S_{yz}=S$. The failure indices have been evaluated at all the layers of the adhesively bonded T-joint. Similar to the stress analysis, the failure indices are found to be more prominent at (i) the interface layer of the flange and web and (ii) 1st layer of the flange, as shown in Figure 3(a) and (b), respectively. As the failure index at the interface layer of the flange and web of the laminated joint structure is maximum compared to the other layers, the adhesion failure may initiate in the same location.

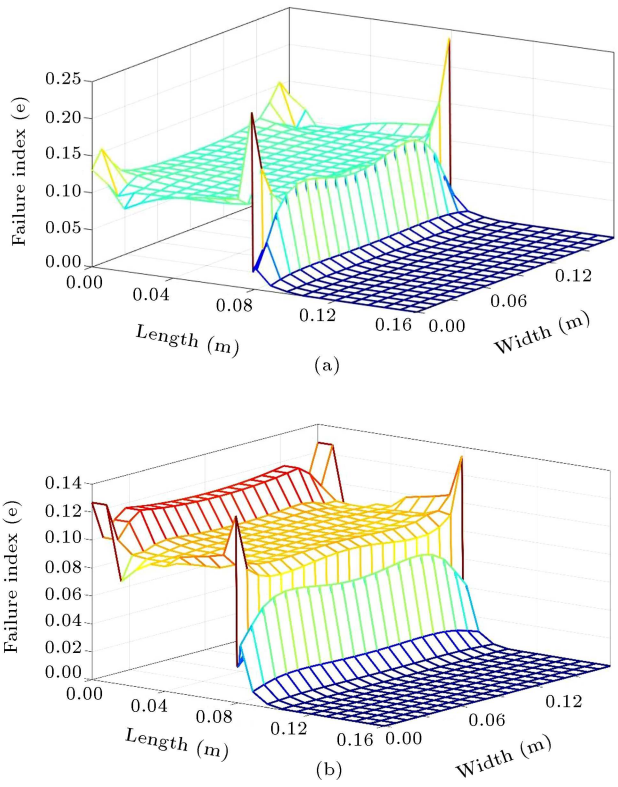

Figure 3. Distribution of failure index: (a) Interface of the flange and web and (b) bottom to interface layer (1st layer of the flange).

3. Adhesion failure analysis

As per the failure analysis, the adhesion failure would initiate at the interface layer of the flange and web part of the laminated T-joint structure. Accordingly, adhesion failure lengths (i.e., 0.0006 m, 0.0012 m, and 0.0018 m) have been pre-embedded in the joint structure (Figure 4). SERRs (G_I, G_{II}, and G_{III}) have been evaluated using Virtual Crack Closure Technique (VCCT) principle to analyze the adhesion failure propagation.

The adhesion failure interface between the web and flange has been provided with duplicate nodes. Multi Point Constraint (MPC) elements are used along the damage front to extract the nodal forces responsible to close the damage. They have been used to connect the corresponding nodes (to constraint) at the interface where no failure occurs. The progressive propagation

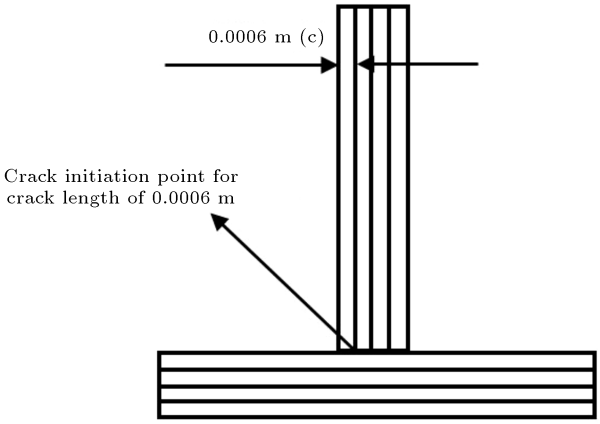

Figure 4. Schematic diagram of the laminated T-joint structure with adhesion failures.

of adhesion failure of varying sizes (c = 0.0006 m, 0.0012 m, and 0.0018 m) has been simulated by detaching the constraints along the interface laminates. Nodal forces required for SERR calculation of adhesion failure are evaluated using these MPC elements. In the adhesion failure region, the corresponding nodes of the interface layers are connected by CONTA178 elements to prevent interpenetration of the layers.

3.1. Calculation of SERRs using VCCT method

According to Irwin's [44] crack closure method, the amount of energy required to close the crack is identical to that of energy released during the crack propagation.

$$\Delta E = \frac{1}{2}\left(X_{1i}.\Delta u_{2i} + Z_{1i}.\Delta w_{2i}\right), \tag{3}$$

where X_{1i} and Z_{1i} represent the nodal forces at point i for shear and opening modes, as shown in Figure 5(a). Similarly, Δu_{2i} and Δw_{2i} represent the difference concerning nodal displacements in shear and opening modes at node i, as shown in Figure 5(b).

The nodal forces obtained at the node point of the finite element model along the failure plane, when multiplied with the face displacements due to adhesion failure along the failure plane, will give the energy-based stress equation.

According to VCCT principle [45], the SERRs for different modes of failure and the total SERR can be calculated through the following equations:

$$G_I = \frac{1}{2\Delta A} Z_f \left(w_T - w_B\right), \tag{4}$$

$$G_{II} = \frac{1}{2\Delta A} X_f \left(u_T - u_B\right), \tag{5}$$

$$G_{III} = \frac{1}{2\Delta A} Y_f \left(v_T - v_B\right), \tag{6}$$

$$G_T = G_I + G_{II} + G_{III}, \tag{7}$$

where G_I, G_{II}, and G_{III} are the SERR values for Modes I, II and III of failures, respectively. Similarly, G_T is the total SERR. The virtually closed area $(\Delta A) = \Delta c \times \Delta c$ and Z_f, X_f, and Y_f represent the nodal forces for the opening, sliding, and tearing modes, respectively. The magnitude of the nodal forces can be calculated using the MPC elements. Crack propagation is prevented using these nodal forces as they hold on the crack tip along the crack front.

4. Use of smart piezoelectric materials

For structural health monitoring technology, the use of piezoelectric material is one of the most popular materials. Smart laminated composites containing piezoelectric active layers have self-actuation and sensing capabilities which can improve the performance of existing laminated composite structures. The analysis schemes of laminated piezoelectric structures are the same as those of the laminated composite structures. The objective of the present work is to develop a coupling analysis model to evaluate the SERR responses for the laminated composite T-joint with single/multiple piezoelectric layers.

Here, the piezoelectric layer has been combined with the layers of the base material in both the flange and web part of the structure. The schematic diagram for one of the cases of the laminated T-joint structure attached to piezoelectric material in the web part is shown in Figure 6.

The effects of single/multiple piezoelectric layers and their suitable locations in the T-joint structure have also been investigated in detail. So, this will

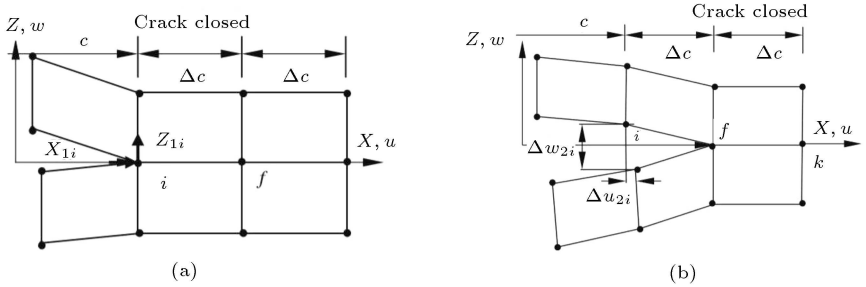

Figure 5. 2D crack closure method: (a) 1st step – crack closed and (b) 2nd step – extended crack length.

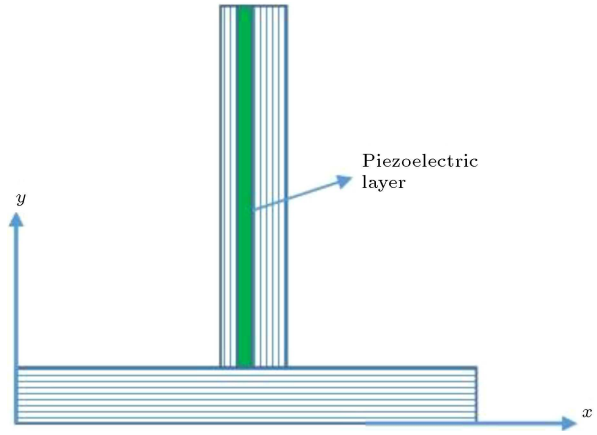

Figure 6. Schematic diagram of the laminated smart T-joint structure.

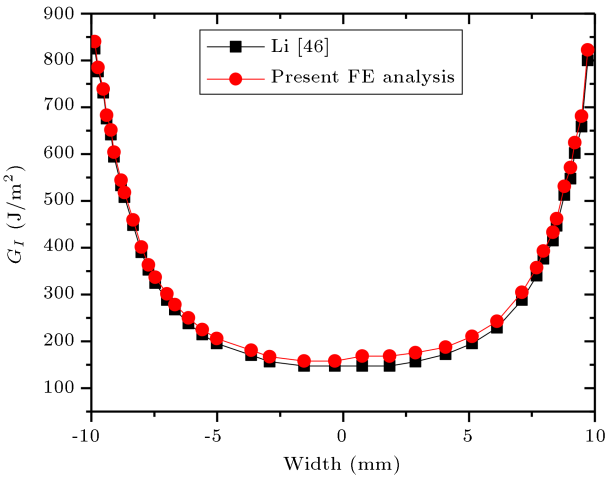

Figure 7. Comparison and validation study.

improve the structural resistance against the adhesion failure propagation of the T-joint structure, as discussed in the result and discussion section.

5. Results and discussion

5.1. Convergence and validation study

To validate the proposed model, a double cantilever beam is considered, for which analytical results are available in the open literature [46]. The double cantilever beam with delamination is subjected to displacement loading in the thickness direction. The SERR obtained for Mode I failure in the double cantilever beam has been compared by keeping the geometrical and material parameters the same as those of the reference. The results predicted by the present model are comparable to those reported by Li [46], as shown in Figure 7.

The accuracy of any numerical model results largely depends on the mesh size. For this, the convergence study of the present T-joint finite model

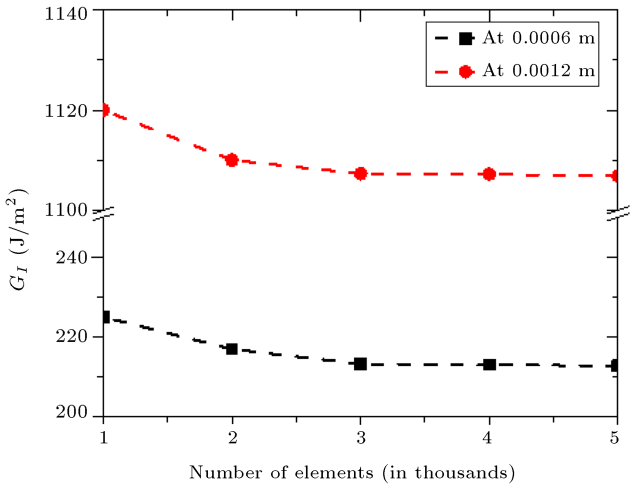

Figure 8. Convergence study of the T-joint joint structure for Mode I (G_I) failure.

has been carried out for the SERR values (G_I, G_{II}, and G_{III}). All these SERR values have been calculated at adhesion failure lengths of 0.0006 m and 0.0012 m of the adhesively bonded T-joint structure. Therefore, the present finite element model has been divided into a number of elements until the convergence of the output results is achieved. From Figure 8, the converged solution of the SERR (G_I) value is obtained for the element size of 3080. Accordingly, further analysis of the T-joint structure is carried out by keeping this element size constant.

5.2. SERRs distribution in the T-joint

Adhesion failure analysis has been carried out to calculate the SERR values for the adhesively bonded T-joint structure. As discussed in Section 3, different adhesion failure lengths (0.0006 m, 0.0012 m, and 0.0018 m) have been considered. Variation in SERR values along the width of the joint structure is presented in Figure 9. The SERR values for Mode I, Mode II, and Mode III failures at different adhesion failure lengths are shown in Figure 9(a)–(c), respectively. It has been observed that the SERR values are increasing with an increase in adhesion failure length. It is also found that the opening mode of failure (G_I) is more dominating than other two modes (Figure 10). Therefore, the total SERR values are largely influenced by SERR for Mode I. The dominance of Mode I failure is detected due to the out-of-plane loading conditions. However, the variation of SERRs is not self-similar. Figure 10 shows the SERR distribution for all modes of failure at a crack length of 0.0006 m. Therefore, it is essential that the total SERR (G_T) is evaluated at different adhesion failure lengths for the T-joint structure. Figure 11 demonstrates that G_T value increases with an increase in crack length and becomes more critical after a crack length of 0.0012 m.

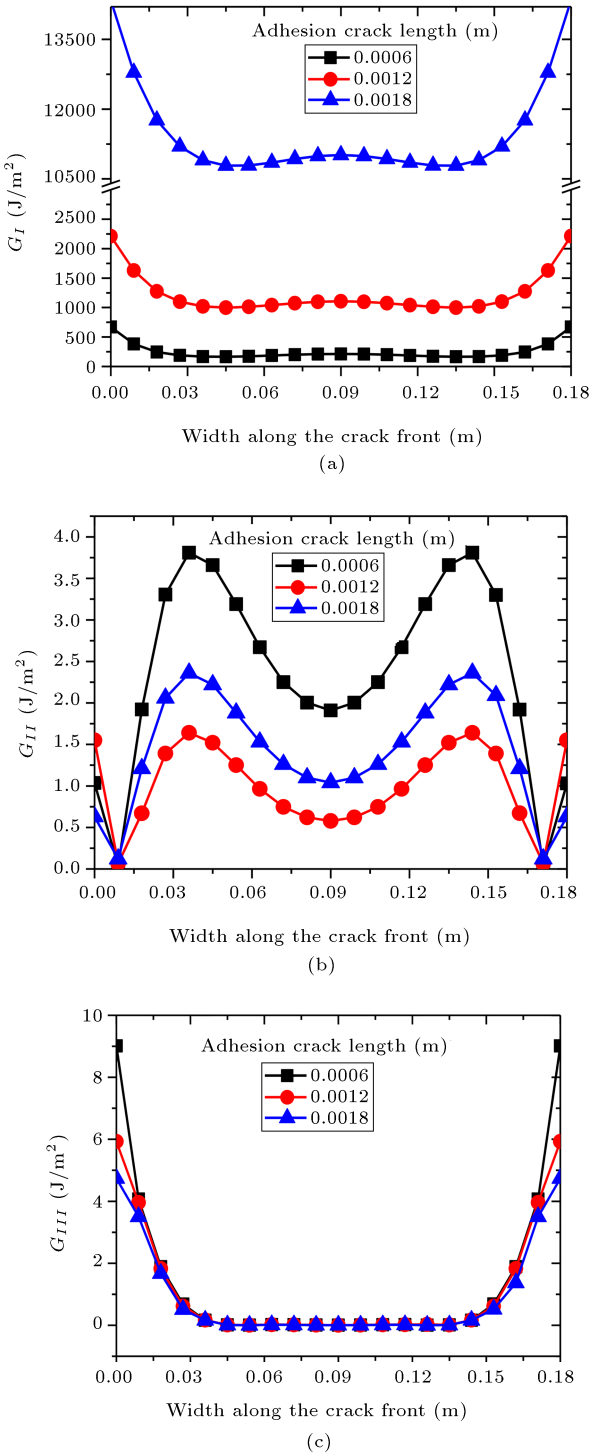

Figure 9. Distribution of Strain Energy Release Rate (SERR) for (a) Mode I (G_I), (b) Mode II (G_{II}), and (c) Mode III (G_{III}) failures at different adhesion failure lengths.

5.3. SERRs distribution in the T-joint with piezoelectric layer

In this section, the behavior of the adhesively bonded composite T-joint structure attached to single/multiple piezoelectric layers at different locations is studied.

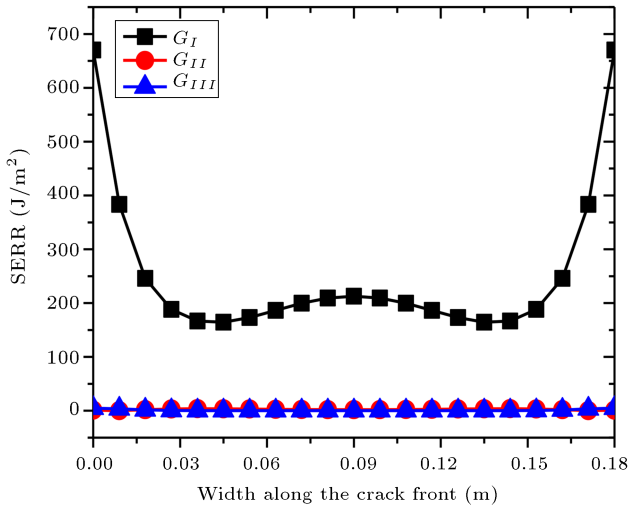

Figure 10. Distribution of Strain Energy Release Rate (SERR) at crack length of 0.0006 m for mode-I, mode-II, and mode-III failures.

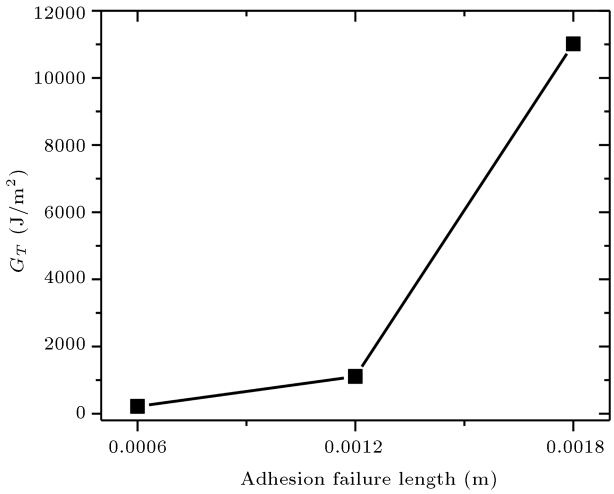

Figure 11. Variation of total SERR (G_T) along the adhesion failure front for different crack lengths.

The laminated T-joint structure attached to piezoelectric layers at different locations for the crack length of 0.0006 m is shown in Figure 12. A similar method was adopted to model the smart structure for the other two crack locations. The SERR values were calculated for all these cases and compared with the original laminated T-joint structure. The piezoelectric material properties considered for the present analysis are shown in Table 5. In the present case, the open-circuit boundary condition has been considered and the voltage at the coupling nodes was assigned a zero value. The mode-I SERR values for nine different cases are tabulated in Table 6.

Among all these smart laminated T-joint (with piezoelectric layer) structures, it was identified that the T-type structure in Case 3 had maximum resistance to

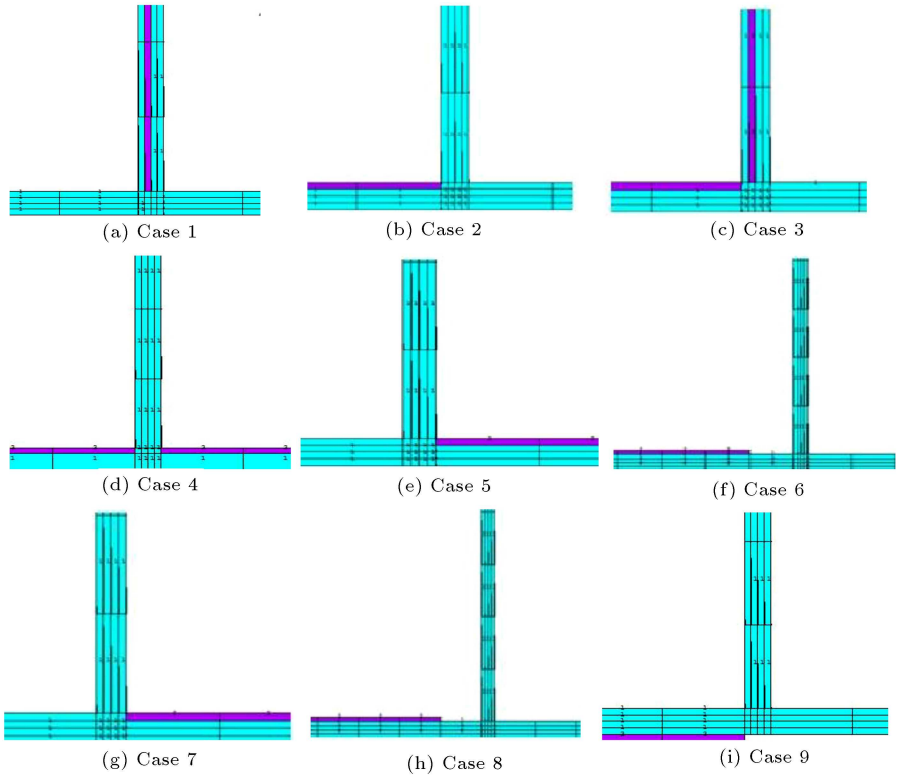

Figure 12. Adhesively bonded T-joint structures with piezoelectric layer in different locations.

Table 5. Material properties of PZT-5H material [47].

Properties	Symbol	PZT-5H
Density (kg/m^3)	ρ	7500
Compliance (10^{-12} m^2/N)	$C_{11} = C_{22}$	16.5
	C_{33}	20.7
	$C_{12} = C_{21}$	–4.78
	$C_{13} = C_{31} = C_{23} = C_{32}$	–8.45
	$C_{44} = C_{55} = C_{66}$	43.5
Piezoelectric coupling (10^{-12} C/N)	$d_{31} = d_{22}$	–274
	d_{33}	593
Relative permittivity ($\varepsilon_T/\varepsilon_o$)	$\varepsilon_{11} = \varepsilon_{22}$	3130
	ε_{33}	3400

crack propagation (Table 5). The smart structure type in Case 3 is a combination of Cases 1 and 2.

The objective to improve the capability of the smart structure against crack propagation was further extended by attaching multiple layers of piezoelectric materials to smart structure types in Cases 1–3. Figure 13 represents an adhesively bonded T-joint structure with multiple piezoelectric layers attached to the type of smart structure in Case 1. Similarly, multiple piezoelectric layers are attached to smart structure types in Cases 2 and 3. A similar trend of responses was obtained for all these cases. Therefore, for the sake of brevity, the SEER values for the Case-1 type of the laminated smart T-joint structure with multiple piezoelectric layers are shown in Figure 14. It was found that there was no significant improvement in resistance to crack propagation with multiple piezoelectric layers in the joint structure for the considered geometry, loading, and boundary conditions.

Table 6. Comparison of Strain Energy Release Rate (SERR) values for Mode I (G_I) failure for different cases.

Case	G_I (J/m^2)
Without PZT	212
Case 1	74
Case 2	183
Case 3	20
Case 4	202
Case 5	202
Case 6	172
Case 7	36
Case 8	216
Case 9	178

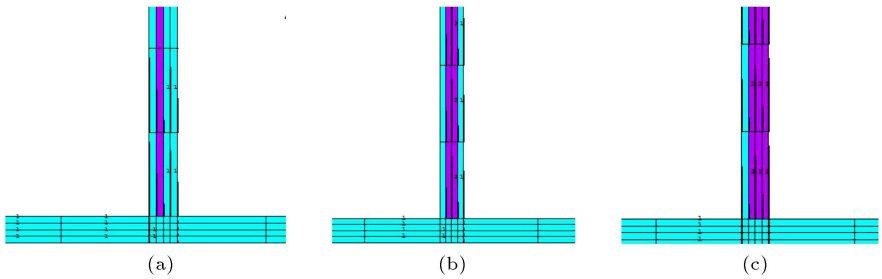

Figure 13. Smart laminated T-joint structure with (a) one, (b) two, and (c) three piezoelectric layers.

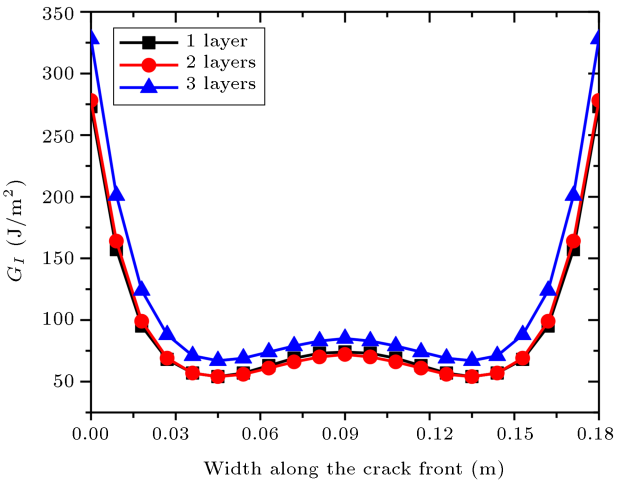

Figure 14. Distribution of SERR (G_I) for the smart laminated joint structure consisting of different numbers of piezoelectric layers.

5.4. Parametric study

In this section, an attempt is made to conduct parametric studies to improve the performance (resistance to adhesion failure) of the laminated smart T-joint structure by considering different orientation schemes, material types, thicknesses, and number of layers of the laminate. All these parametric studies were carried out for the crack length of 0.0006 m in the joint, because similar responses were also obtained for the other two crack lengths.

5.4.1. Orientation scheme

The design of the laminated structures can be easily tailored and stacking orientation is one of the important parameters. Here, unidirectional ply [0/0/0/0], symmetric cross-ply [0/90/90/0], symmetric angle-ply [45/–45/–45/45], and multidirectional ply [0/45/–45/90] orientation schemes for the laminated smart T-joint structure were considered for the purpose of analysis. Table 7 shows the SERR (G_I) values for the different laminated smart T-joint structure. The crack is initiated from the edge of the joint structure. In unidirectional lamina, the fibers are orientated in one direction. Therefore, a crack can easily propagate along the width of the joint structure. As the fiber angle increases, the cracks alone cannot propagate smoothly through the surfaces. Therefore, it is found that the symmetric angle ply lamination scheme for the Case-3 type of laminated smart joint structure exhibits maximum resistance to crack propagation.

Table 7. Variation of SERR (G_I) for different orientation schemes.

Orientation scheme	SERR (G_I (J/m^2))		
	Case 1	Case 2	Case 3
[0/0/0/0]	74.68	183.18	20.69
[0/90/90/0]	74.68	183.18	20.69
[45/–45/–45/45]	21.51	68.34	17.41
[0/45/–45/90]	64.26	114.05	18.91

5.4.2. Laminate material properties

In this section, the effect of laminate material properties on the performance (resistance to adhesion failure) of the laminated smart joint structure is discussed. For this purpose, Carbon/epoxy, Boron/epoxy, E-glass/epoxy, and Graphite/epoxy are considered to model the laminated smart T-joint structure. The material anisotropy of these materials is shown in Table 8. The SERR values for different materials are shown in Table 9. The Case-3 type of laminated smart T-joint structure modeled with E-glass/epoxy material

Table 8. Material anisotropy of different materials [48].

Materials type	E_1/E_2	G_1/G_2
E-glass/epoxy	4.0	9.5
T300/934 carbon epoxy	14.2	21.3
Kevlar/epoxy	14.5	37.0
Graphite/epoxy	46.0	60.0

Table 9. Variation of SERR (G_I) for different composite material properties.

Material type	SERR (G_I (J/m^2))		
	Case 1	Case 2	Case 3
T300/934 carbon epoxy	74.68	183.18	20.69
Graphite/epoxy	137.07	1157.5	35.29
Kevlar/epoxy	133.86	402.88	67.37
E-glass/epoxy	39.08	177.45	5.69

Table 10. Piezoelectric properties of PZT-5A and PZT-4 [49].

Properties	Symbol	PZT-5A	PZT-4
Density (kg/m^3)	ρ	**7750**	**7500**
Compliance (10^{-12} m^2/N)	C_{11}	16.4	12.3
	$C_{22} = C_{33}$	18.8	15.5
	$C_{12} = C_{21}$	–5.74	–4.05
	$C_{13} = C_{31} = C_{23} = C_{32}$	–7.22	–5.31
	$C_{44} = C_{55} = C_{66}$	47.5	39.0
Electric permittivity (10^{-8} F/m)	$\varepsilon_{11} = \varepsilon_{22}$	1.73	1.45
	ε_{33}	1.7	1.3
Piezoelectric strain coefficient (10^{-10} m/V)	$e_{31} = e_{32}$	–1.71	–1.23
	e_{33}	3.74	2.89
	e_{24} = e15	5.84	4.96

exhibits maximum resistance capability. This happens due to the low material anisotropy of E-glass fiber.

5.4.3. Laminate thickness ratio

In this section, different Thickness Ratios (TR) have been considered to understand the thickness effect of the piezoelectric layer on providing resistance to crack propagation. For this purpose, the thickness of the web part of the laminated smart joint structure varied by keeping the thickness of the flange part constant. This will lead to varying thicknesses of the piezoelectric layer in the web part. Other than the original model with the TR of 1, two different TR of 1.5 and 2 were considered. It was found that with an increase in the TR, the SERR value was reduced. This occurred due to the increase in the thickness of the piezoelectric layers, which provided greater resistance to crack propagation by reducing the induced stresses. The SERR variation at different TR is shown in Figure 15.

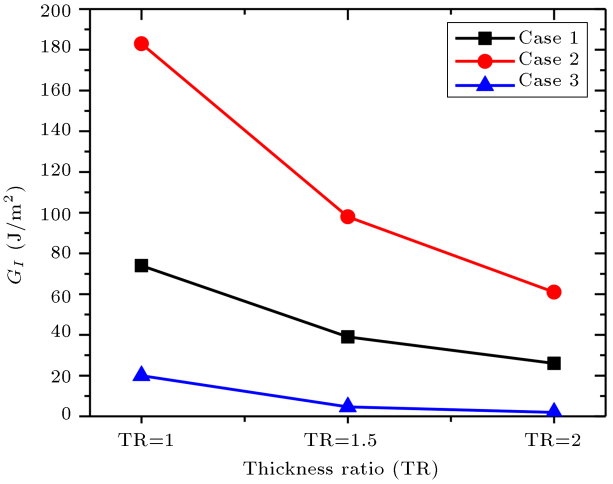

Figure 15. Variation of SERR (G_I) at different thickness ratios.

5.4.4. Piezoelectric materials

Piezoelectric materials play an important role in reducing the SERR in the laminated T-joint structure. For this purpose, three different piezoelectric materials (PZT-5H, PZT-5A, and PZT 4) have been considered. Steady crack growth was observed with PZT materials. Therefore, the effect of different piezoelectric materials was studied. The properties of the piezoelectric materials are shown in Table 10. The lower the G_I value, the higher the resistance to crack propagation. From Figure 16, it is evident that the PZT-5H material type attached to the T-joint structure has lower G_I value than the other two materials. This phenomenon is observed for all the considered cases. This is due to the combined effect of higher piezoelectric co-efficient, relative permittivity, and elastic moduli [50].

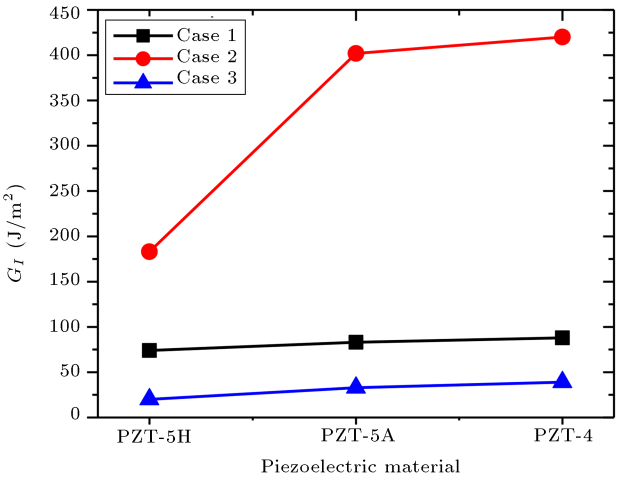

Figure 16. Variation of SERR (G_I) for different piezoelectric materials.

6. Conclusions

Three-dimensional finite element analysis was carried out for the purpose of improving the resistance of the laminated T-joint structure to crack propagation. For this purpose, initially, the stress distributions at the layers of the laminated joint structure were calcu-

lated. By using Tsai-Wu quadratic failure criterion, the location of the crack initiation was evaluated. Further, the Virtual Crack Closure Technique (VCCT) principle was implemented for calculating the Strain Energy Release Rate (SERRs) along the crack front for different adhesion crack lengths. The novelty of this paper lies in the use of piezoelectric material in the laminated T-joint structure. The outcomes of the present analysis are given below:

I. The SERRs for Mode I failure (G_I) were found to be more dominating and responsible for the crack propagation along the crack front of the T-joint structure. The total SERR (G_T) value increased with an increase in the adhesion failure lengths;

II. The use of piezoelectric material as the layer of the laminated T-joint structure significantly reduced the SERRs. Different locations were considered for attaching the piezoelectric material. It was found that the Case-3 type of the laminated smart T-joint structure would provide maximum resistance to crack propagation;

III. Angle ply oriented smart T-joint structure had maximum resistance capability among different types of orientation schemes considered. Similarly, the smart T-joint structure modeled with E-glass/epoxy material as the base material provided maximum resistance to crack propagation. It was found that with an increase in the thickness ratio and the thickness of piezoelectric layers, the resistance of the joint structure to crack propagation was enhanced;

IV. Laminated T-joint structure with a higher piezoelectric coefficient of PZT-5H material provided significant resistance to crack propagation among the other piezoelectric materials considered.

Nomenclature

e	Failure index
S	Inter-laminar shear strength, MPa
Z	Inter-laminar normal strength, MPa
MPC	Multipoint constraint
VCCT	Virtual Crack Closure Technique
SERR	Strain Energy Release Rate
E_x	In-plane elastic modulus, GPa
E_y	In-plane elastic modulus, GPa
E_z	Transverse elastic modulus, GPa
f_{xy}, f_{yz}, f_{xz}	Coupling co-efficient in the principal direction
G_{xy}	In-plane shear modulus, GPa
G_{yz}	Out-of-plane shear modulus, GPa
G_{xz}	Out-of-plane shear modulus, GPa
G_I	Strain energy release rate for mode-I failure, J/m^2
G_{II}	Strain energy release rate for mode-II failure, J/m^2
G_{III}	Strain energy release rate for mode-III failure, J/m^2
G_T	Total strain energy release rate, J/m^2
ν_{xy}	In-plane Poisson's ratio
ν_{yz}	Out-of-plane Poisson's ratio
ν_{xz}	Out-of-plane Poisson's ratio
X_t	Longitudinal tensile strength, MPa
X_c	Longitudinal compressive strength, MPa
Y_t	In-plane tensile strength, MPa
Y_c	In-plane compressive strength, MPa

References

1. Asadijafari, M.H., Zarastvand, M.R., and Talebitooti, R. "The effect of considering Pasternak elastic foundation on acoustic insulation of the finite doubly curved composite structures", *Compos. Struct.,* **256**, pp. 1–11 (2021).

2. Darvish Gohari, H., Zarastvand, M.R., and Talebitooti, R. "Acoustic performance prediction of a multilayered finite cylinder equipped with porous foam media", *JVC/Journal Vib. Control,* **26**(11–12), pp. 899–912 (2020).

3. Talebitooti, R., Zarastvand, M., and Darvishgohari, H. "Multi-objective optimization approach on diffuse sound transmission through poroelastic composite sandwich structure", *J. Sandw. Struct. Mater.*, **23**(4), pp. 1221–1252 (2019).

4. Zarastvand, M.R., Ghassabi, M., and Talebitooti, R. "A review approach for sound propagation prediction of plate constructions", *Arch. Comput. Methods Eng.*, **28**(4), pp. 2817–2843 (2020).

5. Ghassabi, M., Talebitooti, R., and Zarastvand, M.R. "State vector computational technique for three-dimensional acoustic sound propagation through doubly curved thick structure", *Comput. Methods Appl. Mech. Eng.*, **352**, pp. 324–344 (2019).

6. Talebitooti, R., Zarastvand, M.R., and Gohari, H.D. "The influence of boundaries on sound insulation of the multilayered aerospace poroelastic composite structure", *Aerosp. Sci. Technol.*, **80**, pp. 452–471 (2018).

7. Talebitooti, R., Zarastvand, M., and Rouhani, A.S. "Investigating hyperbolic shear deformation theory on vibroacoustic behavior of the infinite functionally graded thick plate", *Lat. Am. J. Solids Struct.*, **16**(1), pp. 1–17 (2019).

8. Zarastvand, M.R., Ghassabi, M., and Talebitooti, R. "Acoustic insulation characteristics of shell structures: A review", *Arch. Comput. Methods Eng.*, **28**(2), pp. 505–523 (2019).

9. Ghassabi, M., Zarastvand, M.R., and Talebitooti, R. "Investigation of state vector computational solution on modeling of wave propagation through functionally graded nanocomposite doubly curved thick structures", *Eng. Comput.*, **36**(4), pp. 1417–1433 (2019).

10. Talebitooti, R. and Zarastvand, M.R. "Vibroacoustic behavior of orthotropic aerospace composite structure in the subsonic flow considering the third order shear deformation theory", *Aerosp. Sci. Technol.*, **75**, pp. 227–236 (2018).

11. Talebitooti, R., Johari, V., and Zarastvand, M. "Wave transmission across laminated composite plate in the subsonic flow investigating two-variable refined plate theory", *Lat. Am. J. Solids Struct.*, **15**(5), pp. 1–20 (2018).

12. Diamanti, K. and Soutis, C. "Structural health monitoring techniques for aircraft composite structures", *Prog. Aerosp. Sci.*, **46**(8), pp. 342–352 (2010).

13. Pagano, N.J. and Schoeppner, G.A. "Delamination of polymer matrix composites: problems and assessment", *Compr. Compos. Mater.*, **2**, pp. 433–528 (2000).

14. Li, D. and Qing, G. "Free vibration analysis of composite laminates with delamination based on state space theory", *Mech. Adv. Mater. Struct.*, **21**(5), pp. 402–411 (2014).

15. Imran, M., Khan, R., and Badshah, S. "Experimental, numerical and finite element vibration analysis of delaminated composite plate", *Sci. Iran.*, **62**(2), pp. 124–134 (2019).

16. Jafari-Talookolaei, R.A., Ebrahimzade, N., Rashidi-Juybari, S., and Teimoori, K. "Bending and vibration analysis of delaminated Bernoulli-Euler microbeams using the modified couple stress", *Sci. Iran.*, **25**(2B), pp. 675–688 (2018).

17. Erturk, A. and Inman, D.J. "On mechanical modeling of cantilevered piezoelectric vibration energy harvesters", *J. Intell. Mater. Syst. Struct.*, **19**(11), pp. 1311–1325 (2008).

18. Lee, J. "Free vibration analysis of delaminated composite beams", *Comput. Struct.*, **74**(2), pp. 121–129 (2000).

19. Tan, P. and Tong, L. "Delamination detection of composite beams using piezoelectric sensors with evenly distributed electrode strips", *J. Compos. Mater.*, **38**(4), pp. 321–352 (2004).

20. Senthil, K., Arockiarajan, A., Palaninathan, R., Santhosh, B., and Usha, K.M. "Defects in composite structures: Its effects and prediction methods - A comprehensive review", *Compos. Struct.*, **106**, pp. 139–149 (2013).

21. Raja, S., Prathima Adya, H.P., and Viswanath, S. "Analysis of piezoelectric composite beams and plates with multiple delaminations", *Struct. Heal. Monit.*, **5**(3), pp. 255–266 (2006).

22. Tang, H.Y., Winkelmann, C., Lestari, W., and La Saponara, V. "Composite structural health monitoring through use of embedded PZT sensors", *J. Intell. Mater. Syst. Struct.*, **22**(8), pp. 739–755 (2011).

23. Patange, S.S.R., Raja, S., Vijayakumar, M.P., and Ranganath, V.R. "Study on low frequency energy harvesting system in laminated aluminum beam structures with delamination", *J. Mech. Sci. Technol.*, **32**(5), pp. 1985–1993 (2018).

24. Vishwas, M., Joladarashi, S., and Kulkarni, S.M. "Comparative study of damage behavior of synthetic and natural ber-reinforced brittle composite and natural ber-reinforced exible composite subjected to low-velocity impact", *Sci. Iran.*, **27**(1), pp. 341–349 (2020).

25. Tan, P. and Tong, L. "Experimental and analytical identification of a delamination using isolated PZT sensor and actuator patches", *J. Compos. Mater.*, **41**(4), pp. 477–492 (2007).

26. Venkata Rao, K., Raja, S., and Munikenche Gowda, T. "Finite element modeling and bending analysis of piezoelectric sandwich beam with debonded actuators", *Smart Struct. Syst.*, **13**(1), pp. 55–80 (2014).

27. Bendenia, N., Zidour, M., Bousahla, A.A., Bourada, F., Tounsi, A., Benrahou, K.H., Bedia, E.A.A., Mahmoud, S.R., and Tounsi., A. "Deflections, stresses and free vibration studies of FG-CNT reinforced sandwich plates resting on Pasternak elastic foundation", *Comput. Concr.*, **26**(3), pp. 213–226 (2020).

28. Allam, O., Draiche, K., Bousahla, A., Bourada, F., Tounsi, A., Benrahou, K.H., Mahmoud, S.R., Adda Bedia, E.A., Tounsi, A. "A generalized 4-unknown refined theory for bending and free vibration analysis of laminated composite and sandwich plates and shells", *Comput. Concr.*, **26**(2), pp. 185–201 (2020).

29. Draiche, K., Bousahla, A.A., Tounsi, A., Alwabli, A.S., Tounsi, A., and Mahmoud, S.R. "Static analysis of laminated reinforced composite plates using a simple first-order shear deformation theory", *Comput. Concr.*, **24**(4), pp. 369–378 (2019).

30. Belbachir, N., Draich, K., Bousahla, A.A., Bourada, M., Tounsi, A., and Mohammadimehr, M. "Bending analysis of anti-symmetric cross-ply laminated plates under nonlinear thermal and mechanical loadings", *Steel Compos. Struct.*, **33**(1), pp. 81–92 (2019).

31. Sahla, M., Saidi, H., Draiche, K., Bousahla, A.A., Bourada, F., and Tounsi, A. "Free vibration analysis of angle-ply laminated composite and soft core sandwich plates", *Steel Compos. Struct.*, **33**(5), pp. 663–679 (2019).

32. Zine, A., Bousahla, A.A., Bourada, F., Benrahou, K.H., Tounsi, A., Bedia, E.A.A., Mahmoud, S.R., and Tounsi, A. "Bending analysis of functionally graded porous plates via a refined shear deformation theory", *Comput. Concr.*, **26**(2), pp. 63–74 (2020).

33. Bourada, F., Bousahla, A.A., Tounsi, A., Adda Bedia, E.A., Mahmoud, S.R., Benrahou, K.H., and Tounsi, A., "Stability and dynamic analyses of SW-CNT reinforced concrete beam resting on elastic-foundation", *Comput. Concr.*, **25**(6), pp. 485–495 (2020).

34. Chikr, S.C., Kaci, A., Bousahla, A.A., Bourada, F., Tounsi, A.A., Bedia, E.A., Mahmoud, S.R., Benrahou, K.H., and Tounsi, A.A. "A novel four-unknown integral model for buckling response of FG sandwich plates resting on elastic foundations under various boundary conditions using Galerkin's approach", *Geomech. Eng.*, **21**(5), pp. 471–487 (2020).

35. Yan, X., Courtney, C.R.P., Bowen, C.R., Gathercole, N., Wen, T., Jia, Y., and Shi, Y. "In situ fabrication of carbon fibre-reinforced polymer composites with embedded piezoelectrics for inspection and energy harvesting applications", *J. Intell. Mater. Syst. Struct.*, **31**(16), pp. 1910–1919 (2020).

36. Kolahchi, R., Hosseini, H., and Esmailpour, M. "Differential cubature and quadrature-Bolotin methods for dynamic stability of embedded piezoelectric nanoplates based on visco-nonlocal-piezoelasticity theories", *Compos. Struct.*, **157**, pp. 174–186 (2016).

37. Ghorbanpour Arani, A., Jamali, M., Mosayyebi, M., and Kolahchi, R. "Wave propagation in FG-CNT-reinforced piezoelectric composite micro plates using viscoelastic quasi-3D sinusoidal shear deformation theory", *Compos. Part B Eng.*, **95**, pp. 209–224 (2016).

38. Motezaker, M., Jamali, M., and Kolahchi, R. "Application of differential cubature method for nonlocal vibration, buckling and bending response of annular nanoplates integrated by piezoelectric layers based on surface-higher order nonlocal-piezoelasticity theory", *J. Comput. Appl. Math.*, **369**, pp. 1–45 (2020).

39. Ghorbanpour-Arani, A.H., Rastgoo, A., Sharafi, M.M., Kolahchi, R., and Ghorbanpour Arani, A. "Nonlocal viscoelasticity based vibration of double viscoelastic piezoelectric nanobeam systems", *Meccanica*, **51**(1), pp. 25–40 (2016).

40. Kolahchi, R., Keshtegar, B., and Fakhar, M.H. "Optimization of dynamic buckling for sandwich nanocomposite plates with sensor and actuator layer based on sinusoidal-visco-piezoelasticity theories using Grey Wolf algorithm", *J. Sandw. Struct. Mater.*, **22**(1), pp. 3–27 (2020).

41. Hajmohammad, M.H., Zarei, M.S., Kolahchi, R., and Karami, H. "Visco-piezoelasticity-zigzag theories for blast response of porous beams covered by graphene platelet-reinforced piezoelectric layers", *J. Sandw. Struct. Mater.*, p. 109963621983917 (2019).

42. Cheuk, P.T. and Tong, L. "Failure of adhesive bonded composite lap shear joints with embedded precrack", *Compos. Sci. Technol.*, **62**(7–8), pp. 1079–1095 (2002).

43. Hahn HT, T.S. "Introduction to composite materials", *Mech. Compos. Mater.*, pp. 1–53 (2018).

44. Irwin, G. "Analysis of stresses and strains near the end of a crack traversing a plate", *J. Appl. Mech.*, **24**, pp. 361–364 (1957).

45. Rybiki, E.F. and Kanninen, M.F. "A finite element calculation of stress intensity factors by a modified crack closure integral", *Eng. Fract. Mech.*, **9**(4), pp. 931–938 (1977).

46. Li, D.H. "Delamination and transverse crack growth prediction for laminated composite plates and shells", *Comput. Struct.*, **177**, pp. 39–55 (2016).

47. Jha, B.K. and Ray, M.C. "Benchmark analysis of piezoelectric bimorph energy harvesters composed of laminated composite beam substrates", *Int. J. Mech. Mater. Des.*, **15**(4), pp. 739–755 (2019).

48. Daniel, I.M., Ishai, O., Daniel, I.M., and Daniel, I. "Engineering mechanics of composite materials", *Mater. Des.*, **17**(2), p. 114 (2006).

49. Hwang, W.S. and Park, H.C. "Finite element modeling of piezoelectric sensors and actuators", *AIAA J.*, **31**(5), pp. 930–937 (1993).

50. Zhang, T. Y., Zhao, M., and Tong, P. "Fracture of piezoelectric ceramics", *Adv. Appl. Mech.*, **38**(C), pp. 147–289 (2002).

Biographies

Subhransu Kumar Panda completed his BSc degree in Mechanical Engineering at National Institute of Science and Technology, Odisha, India. He completed his MSc degree in Mechanical Engineering at CAPGS, BPUT, India. He is currently pursuing his PhD at the Department of Mechanical Engineering, National Institute of Technology, Rourkela, India. His research works are focused on solid mechanics, composites, vibration, and fracture mechanics.

Pradeep Kumar Mishra completed his BSc degree in Mechanical Engineering at Veer Surendra Sai University of Technology, Odisha, India. He completed his MSc degree in Mechanical Engineering at National Institute of Technology, Rourkela, India and received his PhD degree from Indian Institute of Technology, Bhubaneswar, India. He is currently working as an Assistant Professor and HOD at the Department of Mechanical Engineering, CAPGS, BPUT, India. His research interests lies in the field of solid mechanics, vibration, composites, fracture mechanics, and finite element methods.

Subrata Kumar Panda completed his BSc degree in Mechanical Engineering at C.V. Raman College of Engineering, Odisha, India. He completed his MSc degree from the Department of Applied Engineering and Mechanics and Drawing, Bengal Engineering and

Science University, Shibpur (HWH), WB, India and received his PhD degree from Indian Institute of Technology, Kharagpur, India. He is currently working as an Associate Professor at the Department of Mechanical Engineering, National Institute of Technology, Rourkela, India. His research interests are solid mechanics, smart composite structures, FGM, structural optimization, nonlinear finite element methods, etc.